AIAA-2010-5054
10^{th} AIAA/ASME Joint Thermophysics and Heat Transfer Conference, 28 Jun - 1 Jul 2010 , Chicago, Illinois

Knudsen Force Modeling in Application to Microsystems

Jeremy S. Nabeth*, Sruti Chigullapalli*, and Alina A. Alexeenko†
School of Aeronautics & Astronautics, Purdue University, West Lafayette, IN 47907

At the microscale, even moderate temperature differences can result in significant Knudsen forces generated by the energy exchange between gas molecules and solids immersed in a gas. Creating, controlling and measuring Knudsen forces in microsystems can be an arduous task since only limited theory exists at present. This present study investigates the mechanism of Knudsen forces in detail based on numerical solution of the Boltzmann kinetic equation. The Knudsen force is shown, in general, to be a result of thermal non-equilibrium between gas and solid. The simulations are validated by comparison with experimental measurements that have been reported by Passian *et al.*[10] using heated atomic force microscope probes. A closed-form model for the Knudsen force on a beam is obtained based on the simulations and can be applied for analysis and design of microsystems.

I. Introduction

Engineered microsystems have transformed human life in a plethora of ways since their advent in 1990s. The utilization of the fact that at the microscale electrostatic forces can be used to move objects and structures under relatively small applied voltage and power has led to creation of many micro-electro-mechanical systems (MEMS). Micro-cantilevers and fixed-fixed microbeams are some of the most common elements of MEMS-based devices such as pressure sensors, switches and gyroscopes. Knudsen forces arise in such microsystems when there is a thermal gradient with a characteristic length scale comparable to the molecular mean free path of the ambient gas. These forces are also referred to as radiometric or thermo-molecular forces[11] and have been observed experimentally, in example, for heated AFM microcantilevers.[10]

The thermal gradients in microsystems can originate from various reasons, a resistive heating, a laser heating or a difference in optical absorption.[9] Dynamics of microbeams are governed by the combined effect of electrostatic, gas damping and thermal forces. Although Knudsen forces can often be neglected compared to gas damping for devices operating at atmospheric pressures, they can be large at significant temperature gradients and for vacuum-packaged devices. Additionally, Knudsen force in microstructures with thermal gradients can provide a novel actuation mechanism for mass detection, thermogravimetry, and very high-resolution heat flux measurements. The main goal of this paper is to determine the dependence of the Knudsen Force on pressure, geometry and thermal gradients based on rarefied flow simulations.

The remainder of the paper is organized as follow. A description of the phenomenon is given in section II by considering a two-dimensional heated beam separated from a colder substrate. Section III contains details for the numerical model and the accuracy of the solution. Then, in section IV, the computed results are shown and validated with experimental data from Passian *et al.*[10] Finally, a compact model for the Knudsen force is derived in section V and can be used for the design of microsystems.

*Graduate Student, Student Member.
†Assistant Professor, AIAA Member.

II. Knudsen Force on a Two-Dimensional Beam

In typical microsystems, cantilevers and fixed-fixed beams are suspended by a few microns over a substrate. Such configurations are encountered, for example, in microgyroscopes,[8] microaccelerometers[6] and dip pen nanolithography[4] where a temperature gradient between the beam and the substrate can easily be induced.

The phenomenon of Knudsen force can be understood by considering two molecules underneath and above a cantilever microbeam hotter than the substrate. By bringing the beam a few micrometers away from the cold wall, the gradient of gas temperature below the beam is greater than the one above (Fig. II). When hitting the beam, the upper molecule will give its momentum to the beam in the negative y-direction, whereas, the molecule below the beam will give its momentum in the upward direction. Given the difference in temperature gradients, the incident molecule below the beam will be in a colder area since the temperature drops substantially faster. Therefore, while moving toward the beam, the molecule will experience a larger gain in momentum than the one coming from above the beam. Consequently, the resulting momentum given to the beam will be in the direction of positive y-axis and the beam will tend to move upward.

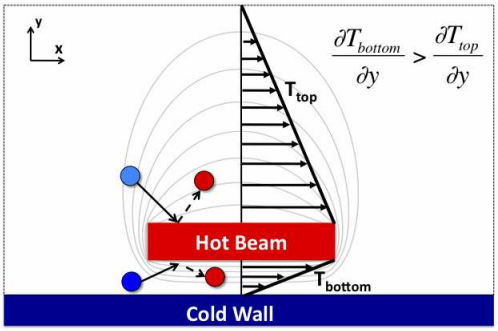

Figure 1. Schematic of domain.

The degree of rarefaction of the gas is quantified by computing the Knudsen number. This dimensionless number is defined as the ratio of the molecular mean-free path to a characteristic length and gives insights into the applicability of different governing equations. In this work, the Knudsen number is based on the variable hard sphere model from Bird.[3] It permits the definition of a mean-free path λ and a Knudsen number that account for the real gas temperature exponent of the coefficient of viscosity.

$$\lambda = \frac{kT}{\sqrt{2}\pi d_{ref}^2 P(\frac{T_{ref}}{T})^{\omega-0.5}}$$
$$Kn = \frac{\lambda}{L}$$

where k is Boltzmann's constant, T is the temperature of the beam, d_{ref} is the diameter of the molecule measured at the reference temperature T_{ref}, ω is the viscosity index, P is the pressure and L is the characteristic length.

By using the symmetry, only the right half of domain in figure II is used for simulations. The three-dimensional problem along with the cross section used for the simulations is shown on figure 2(a). In order to optimize the computation time, the symmetry boundary condition is used and only the right half of the domain is considered (Fig. 2(b)). The left, top, right and bottom boundaries are symmetry, pressure inlet, pressure inlet and wall boundaries respectively. Detailed micro-cantilever geometry and gas flow conditions are listed in table 1.

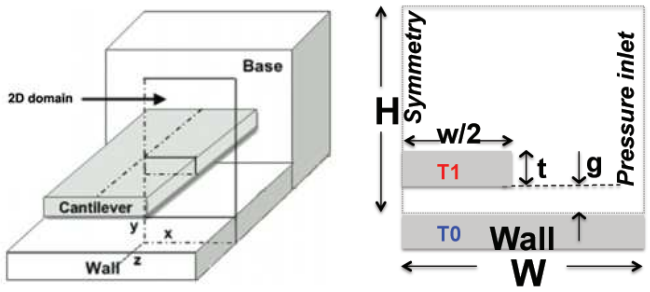

(a) Microbeam near a substrate (b) Two-dimensional simulation setup

Figure 2. Schematics of the configuration

Table 1. Micro-cantilever geometry and flow conditions.

Property	**Symbol**	**Nominal value**
Beam length	L	$200\mu m$
Beam width	w	$20\mu m$
Beam thickness	t	$2\mu m$
Gap size	g	$2\mu m$
Knudsen number	Kn	$0.20 - 10$
Ambient Temperature	T	$300K$
Gas	Ar	Argon
	N_2	Nitrogen
	He	Helium
Temperature Difference	$\Delta T = T_1 - T_0$	$3 - 400K$

III. Numerical Model

The Knudsen force on a 2D heated beam is calculated based on numerical solution of ellipsoidal statistical Bhatnagar-Gross-Krook (ES-BGK) collision model. Details of the formulation and numerical implementation can be found in reference.[2,7] A range of Knudsen number is studied, varying from continuum to free-molecular flow(~ 0.20 to 4). The quasi-steady Boltzmann kinetic model for the velocity distribution function f can be written as

$$u\frac{\partial f}{\partial x} + v\frac{\partial f}{\partial y} = -\nu(f - f_0) \tag{1}$$

where u and v are the gas molecular velocities in the x and y directions, respectively, ν is the collision frequency and f_0 is the equilibrium distribution function.

In the ES-BGK model, f^0 is the local anisotropic Gaussian distribution,

$$\begin{aligned} f^0 &= f_G = \frac{n}{(2\pi)^3 det[\lambda_{ij}]} \cdot exp(-\frac{v_i v_j}{\lambda_{ij}}) \\ \lambda_{ij} &= \frac{1}{Pr} \cdot RT\delta_{ij} + (1 - \frac{1}{Pr}) \cdot p_{ij}\rho \end{aligned}$$

where p_{ij} is the pressure tensor, δ_{ij} is the Kronecker delta and Pr is the Prandtl number.

Assuming that the length of the micro-cantilever is much larger than the width and thickness, the problem simplified to a two-dimensional problem and thus, reduced distribution functions, $f_1 = \int_{-\infty}^{\infty} f dw$ and $f_2 = \int_{-\infty}^{\infty} w^2 f dw$ were used and w is the gas molecular velocity in the z direction.

The solver employs a finite volume method (FVM) with a second order quadrant-splitting scheme applied in the physical space. The velocity space in polar coordinates consisted of 16^{th}-order Gauss-Hermite quadrature in velocity magnitude and 64 uniform velocity angles. Uniform and non-uniform structured meshes were used in the physical phase. In the quasi-steady two-dimensional ES-BGK simulations, Knudsen force is obtained by integrating the computed normal pressure component P_{yy} along the width of the cantilever cross section and the shear pressure P_{xy} along the thickness of the beam as shown in equation (2).

$$\begin{aligned} n &= \int_{-\infty}^{\infty} f_1 dv \\ P_{yy} &= \frac{1}{n}\int_{-\infty}^{\infty} (v')^2 f_1 dv \\ P_{xy} &= \frac{1}{n}\int_{-\infty}^{\infty} u'v' f_1 dv \end{aligned} \tag{2}$$

Grid convergence was verified for physical and velocity space. Figure 3(a) shows the domain size convergence. It can be observed that the height of the domain has a greater influence than the width for values lower than $20\mu m$. When the height is larger than $20\mu m$, the variations stay within 5% of total force. The velocity grid convergence test as shown in 3(b) showed that the number of velocity angles should be larger than 32.

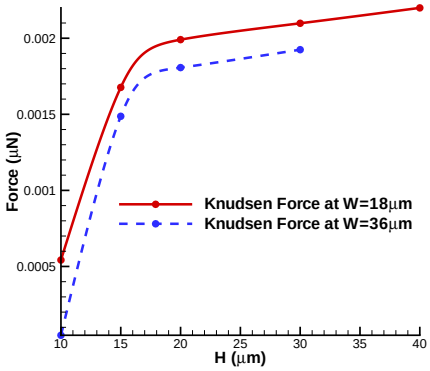

(a) Domain convergence with 64 velocity angles

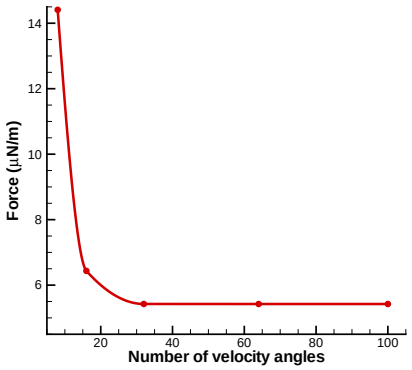

(b) Velocity grid convergence with $W = 18\mu m, H = 10\mu m$

Figure 3. Convergence tests: $Kn = 0.5, \Delta T = 3K, \Delta x = 0.18\mu m, \Delta y = 0.10\mu m$.

In order to optimize the computation time, a non-uniform grid was developed for the physical space. This mesh consists of a uniform grid in the vicinity of the beam and a non-uniform one everywhere else. The non-uniform grid is generated using the following equation,

$$\frac{x_{i+1} - x_i}{x_1 - x_0} = K^i \tag{3}$$

where K is the refinement factor, set to 1.059. A schematic of the mesh is shown on Fig.4, notice that this mesh respects the boundaries of the beam, which reduces the numerical error. Detailed parameters for the three different versions of the mesh are listed in Table 2 with $w = 20\mu m$, $g = 2\mu m$, $t = 2\mu m$, $a = 12\mu m$ and $b = 7\mu m$.

Table 2. Detailed parameters for the mesh.

Designation	Nx_1	Nx_2	Nx_3	Ny_1	Ny_2	Ny_3	Ny_4
$Mesh_1$	75	15	45	30	30	30	45
$Mesh_2$	100	20	60	40	40	40	60
$Mesh_3$	125	25	75	50	50	50	75

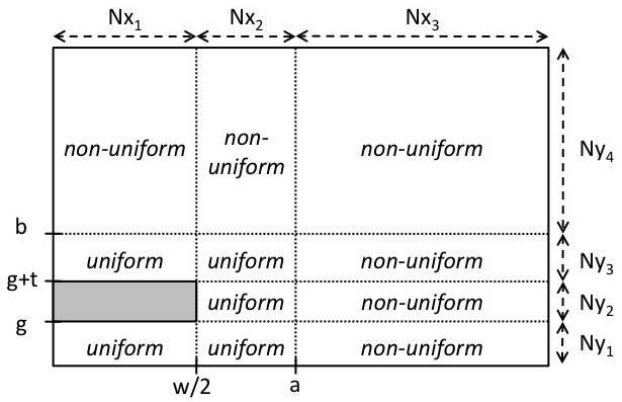

Figure 4. Schematic of the Mesh.

The Richardson Extrapolation[1] has been used in order to quantify the accuracy of the code. Assuming that the discrete solution $F(h)$ is a continuous and differentiable function of a representative mesh size h, it has a series representation:

$$F(h) = F_{exact} + C_k h^k + O(h^{k+1}) \tag{4}$$

Therefore, we can combine solutions on different meshes to eliminate the leading error terms. Let r be the refinement factor between the meshes.

$$\begin{aligned} RE^k(F(h), F(h/r)) &= \frac{r^k F(\frac{h}{r}) - F(h)}{r^k - 1} = F_{exact} + O(h^{k+1}) \\ RE^k(F(h), F(\frac{h}{r_1}), F(\frac{h}{r_2})) &= \frac{\alpha_2 RE^k(F(h), F(\frac{h}{r_1})) - \alpha_1 RE^k(F(h), F(\frac{h}{r_2}))}{\alpha_2 - \alpha_1} = F_{exact} + O(h^{k+2}) \\ \alpha_i &= (r_i(r_i^{k-1} + r_i^{k-2} + ... + 1))^{-1}, i = 1, 2 \end{aligned} \tag{5}$$

Table 3. Richardson extrapolation from three different mesh sizes.

Discrete Solution	**Total Force** ($\mu N/m$)	**Estimated Error** (%)	**Computational time** ($hour$)
$Mesh_1$	62.5	40.52	40.3
$Mesh_2$	74.4	29.19	83.4
$Mesh_3$	83.0	21.01	137.6
$Re(1,2)$	89.7	14.63	
$Re(1,3)$	94.5	10.03	
$Re(2,3)$	98.3	6.46	
$Re(1,2,3)$	100.5	-	

The error in Knudsen force based on 3 different meshes is shown in table 3. In order to keep a reasonable computation time while reducing the numerical error, $Re(2,3)$ is used for the simulations, giving a numerical error of 6.46%.

IV. Results and Validation

The computed flowfields are shown in Fig. 5 for the case of argon gas at a Knudsen number of $Kn = 0.45$ and $Kn = 5$ at ΔT=30K. One can see the creation of a vortex at the corner of the beam resulting in an upward force. The temperature contours are shown in Fig. 6, the uniformity of temperature in the vicinity of the beam at Kn=5 results in a smaller Knudsen force than the one computed at Kn=0.45.

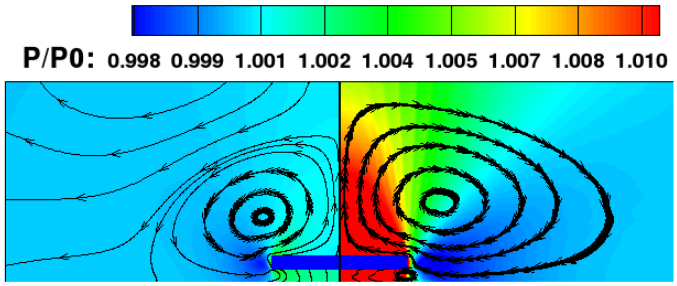

Figure 5. Computed non-dimensional pressure at Kn=0.45 (left) and Kn=5 (right).

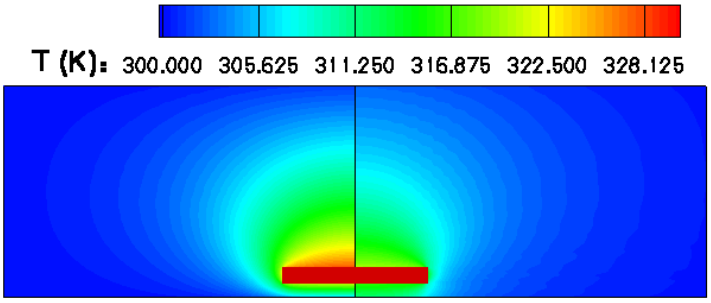

Figure 6. Computed Temperature at Kn=0.45 (left) and Kn=5 (right).

Figure 7 shows the gradients of temperature below and above the beam for two different Knudsen numbers. As expected with the qualitative approach the gradient of temperature is larger below the beam in both cases. The ratio of temperature gradient below and above the beam is 3.75 at Kn = 0.45 and reduces to 1.35 when Kn = 5.

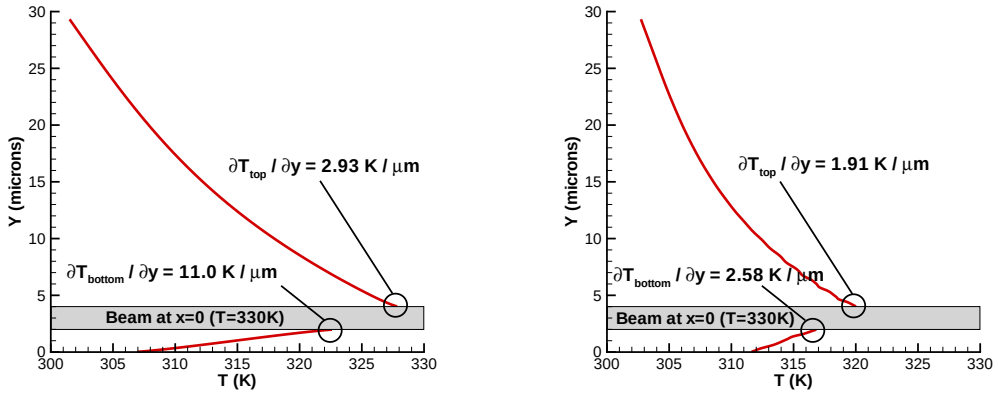

(a) Kn = 0.45 (b) Kn = 5

Figure 7. Temperature Profile at $\Delta T = 30K$

The pressure profiles on figure 8 clearly show that the pressure on the bottom of the beam is larger than the one on the top. Thus, the resulting force on the beam is upward which agrees with the qualitative approach. Moreover, one can see that the lateral pressure is much smaller than the normal pressure and therefore does not have a large impact on the total force.

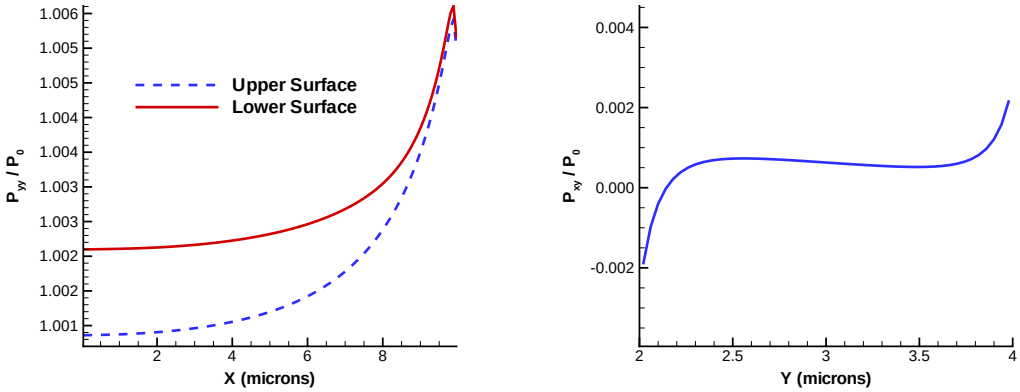

(a) Normal Pressure at Kn = 0.45

(b) Lateral Pressure at Kn = 0.45

Figure 8. Pressure Profile at $\Delta T = 30K$

For a constant gap size, reducing the pressure leads to an increase of the mean-free path and therefore an increase of the Knudsen number. Figure 9 shows the velocity contours and the streamlines of the gas for various Knudsen numbers. One can notice the increase of the size of the vortex that is created at the edge of the beam.

The simulations have been compared with experimental results from Passian *et. al.*[10] In his experiments, a surface-micromachined cantilever was heated by focused illumination with a 529nm line of an argon ion laser. By modulation of the laser frequency, the temperature difference between the cantilever and the substrate remained constant. In order to simulate this three-dimensional configuration with the two-dimensional code, the front-to-side ratio of 0.1 was preserved along with the temperature difference of $\Delta T = 30K$. The simulations agree with the experimental results for both argon and nitrogen (Fig. 10(a) and 10(b)) with a maximum deviation of 3.7% for argon and 9.0% for nitrogen, both at $Kn = 0.4$ and an accommodation coefficient of 1. As shown on fig. 10(c), an accommodation coefficient of 0.8 leads to a closer match with the experimental results than an accommodation coefficient of 1.

V. Compact Model for the Knudsen Force

Based on the simulations, a closed-form expression for Knudsen force on a heated beam at a distance g from a substrate at temperature T_0 for a gas with density ρ, ratio of specific heats γ and gas constant R is developed. The dynamic similarity analysis,[5] results in the following non-dimensional relation:

$$C_{Kn} = \frac{F'_{Kn}}{\rho R \Delta T w} = f(\frac{T_0}{\Delta T}, Kn, \frac{t}{g}, \frac{w}{g}, \gamma, \alpha_t) \tag{6}$$

where C_{Kn} is the Knudsen force coefficient, F'_{Kn} is the force per unit length on the beam, ΔT is the temperature difference between the beam and the substrate, Kn is the Knudsen number, t and w are the thickness and width of the beam, respectively, γ is the heat capacity ratio and α_t is the momentum accommodation coefficient for the gas.

Equation 6 can be further reduced by considering a cantilever with large aspect-ratio. Indeed, when the thickness of the beam is small compared to its width, the integrated pressure on the side can be neglected when computing the total force. Moreover, in most cases the momentum accommodation coefficient is equal to one.

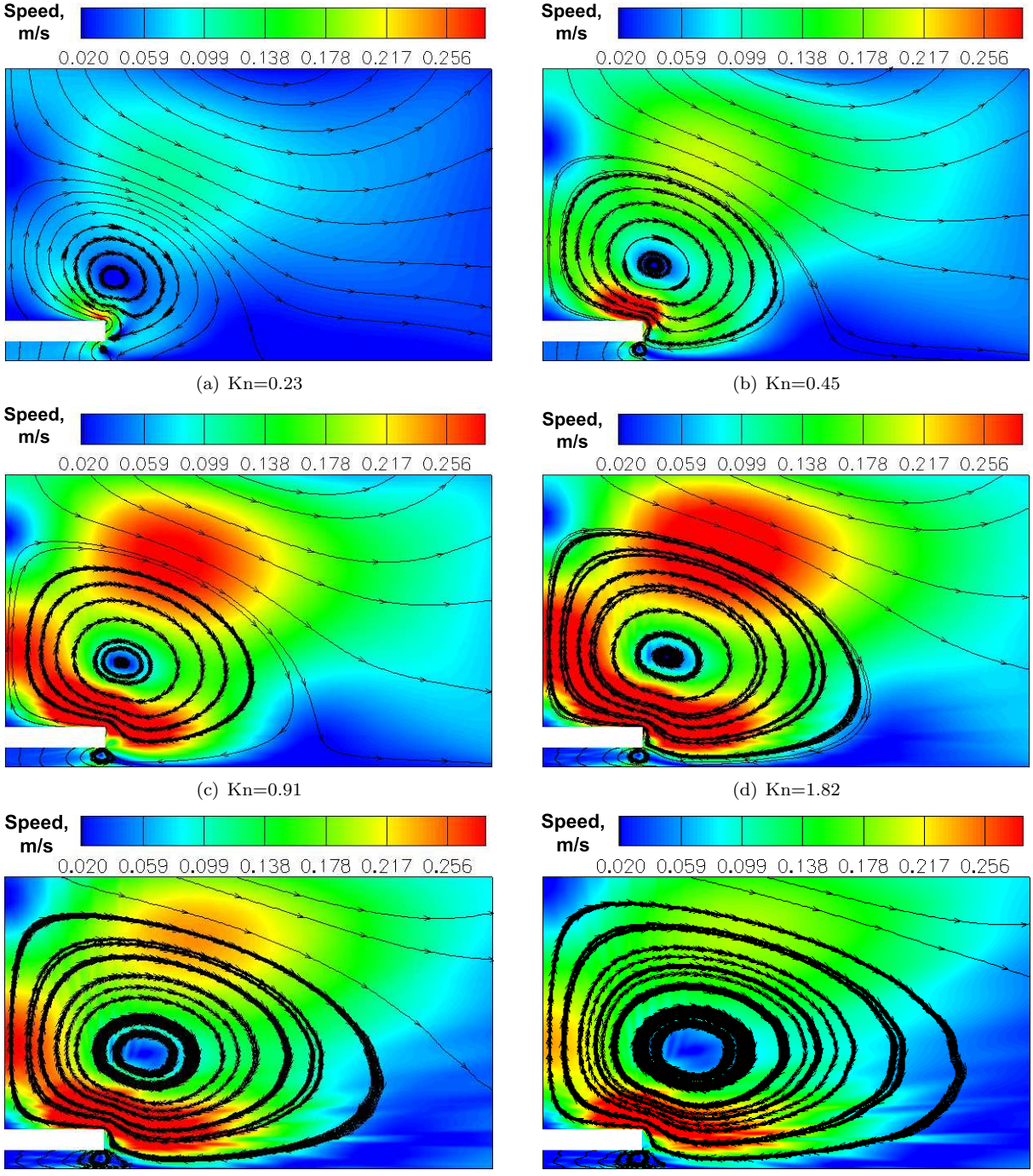

(a) Kn=0.23

(b) Kn=0.45

(c) Kn=0.91

(d) Kn=1.82

(e) Kn=4

(f) Kn=6

Figure 9. Effect of Knudsen number on the flowfields

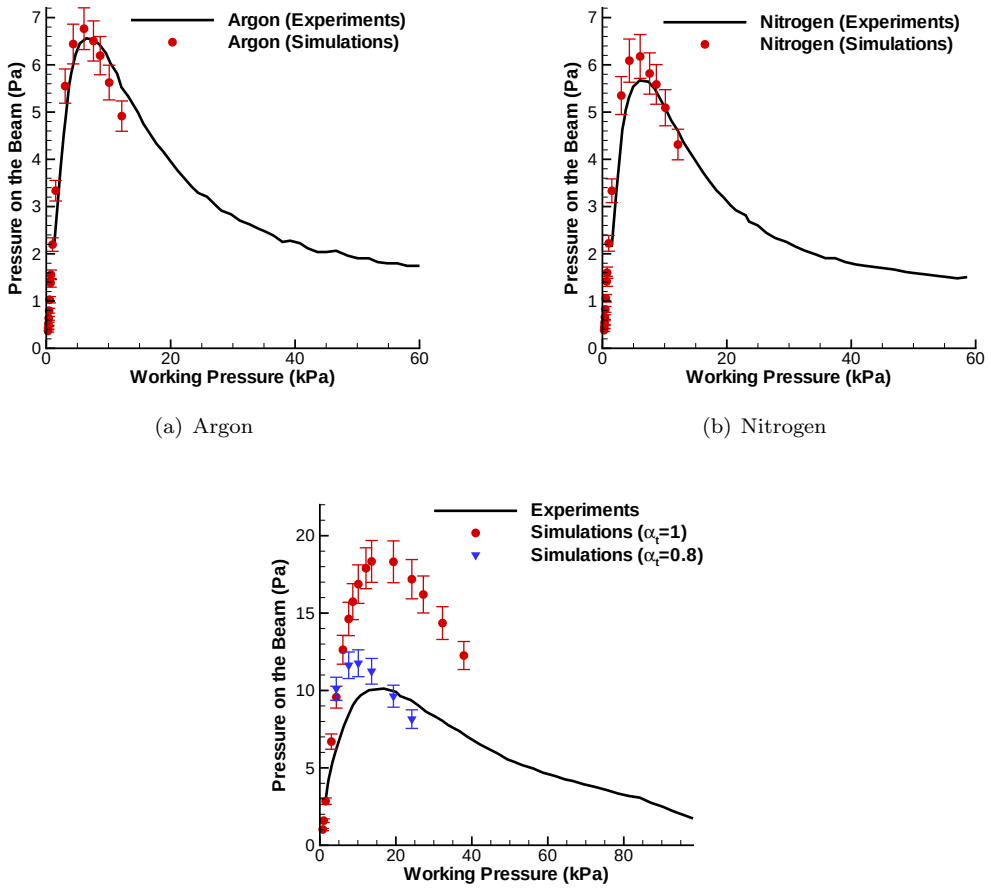

(a) Argon

(b) Nitrogen

(c) Helium

Figure 10. Comparison of Knudsen force simulations with experimental data from Passian *et al.*[10]

Hence, eqn. 6 can be reduced to:

$$C_{Kn} = \frac{F'_{Kn}}{\rho R \Delta T w} = f(\frac{T_0}{\Delta T}, Kn, \frac{w}{g}) \tag{7}$$

The least mean squares algorithm was used to derive an equation for the simulation results. The expression for the Knudsen force coefficient based on Kn is:

$$C_{Kn} = \frac{1}{AKn^{\alpha} + BKn^{\beta} + CKn^{\gamma}} \tag{8}$$

where $A = 38.0535, B = 5.6832, C = 8.3818, \alpha = -0.3835 \beta = -2.3362$, and $\gamma = 0.8549$.

The influence of $\frac{T}{\Delta T}$ has been investigated by setting the Knudsen number to two and running simulation for $\frac{T}{\Delta T}$ ranging from 0.75 to 60 (Fig.11(b)). The deviation from $\frac{T}{\Delta T} = 10$, which correspond to the value at which equation 8 was derived, is then used to obtain an expression for a correction factor.

$$\alpha_{Kn_1} = D_1(\frac{T}{\Delta T})^{\delta_1} + E_1(\frac{T}{\Delta T})^{\epsilon_1} \tag{9}$$

where $D_1 = -0.9146, E_1 = 0.6203, \delta_1 = -0.4224$, and $\epsilon_1 = -0.2602$.

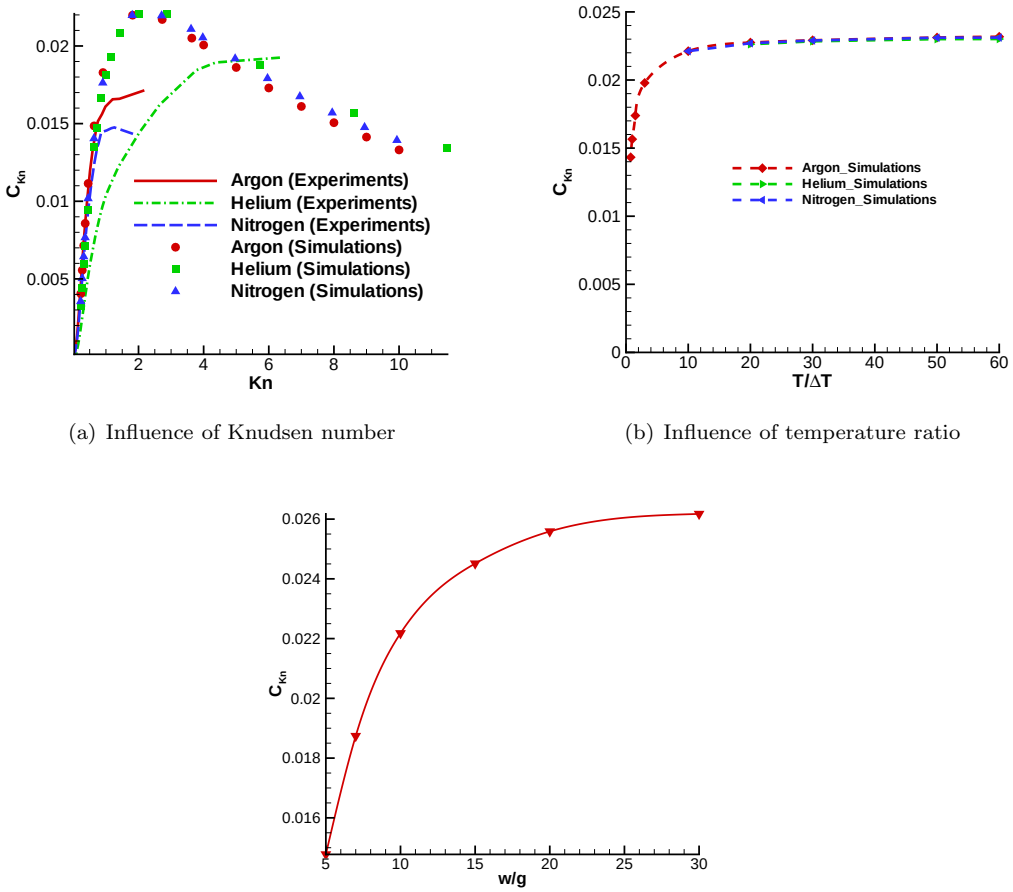

(a) Influence of Knudsen number

(b) Influence of temperature ratio

(c) Influence of beam aspect ratio

Figure 11. Force coefficient from simulations and experiments.

The effect of $\frac{w}{g}$ is obtained by running simulations for $Kn = 2$ and $\frac{T}{\Delta T} = 10$. An expression for the correction factor is obtained by measuring the deviation between the compact model and the simulation results.

By using the least mean squares algorithm, the following expression is obtained,

$$\alpha_{Kn_2} = D_2(\frac{w}{g})^{\delta_2} + E_2(\frac{w}{g})^{\epsilon_2} \tag{10}$$

where $D_2 = -4.0798, E_2 = 0.9511, \delta_2 = -0.9019$, and $\epsilon_2 = -0.2609$.

When including both correction factors, the equation for the Knudsen force coefficient becomes,

$$C_{Kn} = \frac{(1 + D_1(\frac{T}{\Delta T})^{\delta_1} + E_1(\frac{T}{\Delta T})^{\epsilon_1}) \cdot (1 + D_2(\frac{w}{g})^{\delta_2} + E_2(\frac{w}{g})^{\epsilon_2})}{AKn^{\alpha} + BKn^{\beta} + CKn^{\gamma}} \tag{11}$$

The statistical tests examine the goodness-of-fit of the model. A summary of the statistical analysis is listed on table V and shows that:

- The model has high fidelity (chi-square test)
- The relative trend magnitudes are well captured (Pearson's r^2)
- The model predictions are close to observations (Root mean square deviation and mean absolute deviation)

Table 4. Constants for the Compact Model

Constant name	Value	Constant name	Value
A	38.0535	α	-0.3835
B	5.6832	β	-2.3362
C	8.3818	γ	0.8549
D_1	-0.9146	δ_1	-0.4224
E_1	0.6203	ϵ_1	-0.2602
D_2	-4.0798	δ_2	-0.9019
E_2	0.9511	ϵ_2	-0.2609

Table 5. Statistical Analysis of the ESBGK-based compact model

Property	Symbol	Value
Chi-square test	χ^2	1.8696×10^{-5}
Pearson's r^2	r^2	0.9996
Root mean square deviation	RMSD	1.0795×10^{-4}

$$\chi^2 = \sum_{i=1}^{N} \frac{(y_i - x_i)^2}{\sigma_i^2}$$

$$r^2 = 1 - \frac{\sum_{i=1}^{N}(y_i - x_i)^2}{\sum_{i=1}^{N}(y_i - \bar{y}_i)^2}$$

$$RMSD = \sqrt{\frac{\sum_{i=1}^{N}(y_i - x_i)^2}{N}}$$

VI. Conclusion

In this work, we investigated the Knudsen forces in microsystems using rarefied flow simulations. The numerical approach is based on the discrete ordinate and finite volume solution of ESBGK equations. The simulation results proved that the Knudsen force is a result of a non-equilibrium thermal transport. The study showed that the two-dimensional numerical modeling of argon and nitrogen agree well with measurements whereas the measurements for helium are lower than the simulation predictions due to incomplete momentum accommodation. The closed-form correlation for Knudsen force dependence on pressure, geometry and temperature difference can be used for design and analysis of microsystems.

References

[1]A. A. Alexeenko. Numerical Error Analysis for Deterministic Kinetic Solutions of Low-Speed Flows. In *25th International Symposium on Rarefied Gas Dynamics*, pages 184–196, Saint-Petersburg, Russia, 2007.

[2]A.A. Alexeenko, S.F. Gimelshein, E.P. Muntz, and A.D. Ketsdever. Kinetic Modeling of Temperature-Driven Flows in Short Microchannels. *International Journal of Thermal Sciences*, 45(11):1045–1051, 2006.

[3]G. A. Bird. *Molecular Gas Dynamics and the Direct Simulation of Gas Flows*. Oxford University Press, New York, 2nd revised edition edition, 1994.

[4]D. Bullen, X. Wang, J. Zou, S.W Chung, C. Mirkin, and C. Liu. Design, fabrication, and characterization of thermally actuated probe arrays for dip pen nanolithography. *J. MEMS*, 13(4):594–602, 2004.

[5]W.D Curtis, J.D. Logan, and W.A. Parker. Dimensional Analysis and the Pi Theorem. *Linear Algebra and Applic*, 47(10):117–126, 1982.

[6]J. H. Daniel and D.F. Moore. A microaccelerometer structure fabricated in silicon-on-insulator using a focused ion beam process. *Sensors and Actuators*, 73:201–209, 1999.

[7]L.H. Holway Jr. New statistical models for kinetic theory: methods of construction. *Physics of fluids*, 9:1658, 1966.

[8]S. Lee, S. Park, J. Kim, S. Lee, and D. Cho. Surface/Bulk Micromachined Single-Crystalline-Silicon Micro-Gyroscope. *J. MEMS*, 9:557–567, 2000.

[9]B. A. Nelson and W. P. King. 30 Applications of Heated Atomic Force Microscope Cantilevers. In *Applied Scanning Probe Methods IV*, pages 251–275, Berlin, Heidelberg, 2006. Springer.

[10]A. Passian, R. J. Warmack, T. L. Ferrell, and T. Thundat. Thermal Transpiration at the Microscale: A Crookes Cantilever. *Physical Review Letters*, 90(12):124503–1–4, 2003.

[11]L. M. Phinney, J. R. Serrano, E. S. Piekos, J. R. Torczynski, M. A. Gallis, and A. D. Gorby. Raman Thermometry and Thermal Simulations for MEMS Bridges at Pressure from 0.05 to 625 Torr. In *2009 ASME Summer Heat Transfer Conference*, pages HT2009–88583, San Fransisco, California, 2009.